Pseudoresonant Laser Wakefield Acceleration Driven by 10.6-μm Laser Light

W. D. Kimura, *Senior Member, IEEE*, N. E. Andreev, M. Babzien, I. Ben-Zvi, D. B. Cline, C. E. Dilley, S. C. Gottschalk, S. M. Hooker, K. P. Kusche, S. V. Kuznetsov, I. V. Pavlishin, I. V. Pogorelsky, A. A. Pogosova, L. C. Steinhauer, A. Ting, V. Yakimenko, A. Zigler, and F. Zhou

***Abstract*—This paper describes an experiment to demonstrate, for the first time, laser wakefield acceleration (LWFA), driven by 10.6-μm light from a CO_2 laser. This experiment is also noteworthy because it will operate in a pseudoresonant LWFA regime, in which the laser-pulse-length is too long for resonant LWFA, but too short for self-modulated LWFA. Nonetheless, high acceleration gradients are still possible. This experiment builds upon an earlier experiment called staged electron laser acceleration (STELLA), where efficient trapping and monoenergetic laser acceleration of electrons were demonstrated using inverse free electron lasers. The aim is to apply the STELLA approach of laser-driven microbunch formation followed by laser-driven trapping and acceleration to LWFA. These capabilities are important for a practical electron linear accelerator based upon LWFA.**

***Index Terms*—Capillary discharge, carbon dioxide lasers, electron accelerators, laser accelerators, laser wakefield acceleration.**

I. Introduction

A NUMBER of different mechanisms are being investigated around the world to develop electron linear accelerators driven either directly or indirectly by laser light; see examples in [1]. High acceleration gradients > 1 GeV/m have been demonstrated; thus, laser-driven accelerators (laser linacs) may someday enable compact, potentially less expensive accelerators.

However, acceleration of useful amounts of charge requires efficiently grouping the electrons into a microbunch(es), and trapping the microbunch(es) in the ponderomotive potential well ("bucket") of the accelerating wave. This can be an electromagnetic wave, such as in inverse free electron lasers (IFELs) [2], or a plasma wave, such as in laser wakefield acceleration (LWFA) [3]. Having a narrow energy spread of the accelerated electrons (i.e., monoenergetic) is also important for efficient trapping and is often required by many applications.

Generally, these mechanisms have practical limits to the maximum length of the acceleration regions. For example, gradual phase slippage can occur between the accelerating wave and the accelerated electrons. Hence, it will be necessary to repeat the acceleration process by staging multiple laser-driven acceleration sections. This implies the need to resynchronize the phase of the trapped electrons with the accelerating wave in these stages.

This process of trapping and staging is exactly analogous to the method utilized in microwave-driven accelerators. A key difference is the wavelength of the accelerating wave in laser-driven devices may be of order one to several hundred microns instead of centimeters.

Most laser acceleration research has focused on studying specific acceleration processes. The staged electron laser acceleration (STELLA) experiment [4] was specifically designed to demonstrate efficient trapping and staging of laser-driven acceleration devices. STELLA used IFELs, which were chosen primarily for experimental convenience. In fact, the overall STELLA approach can be applied to other acceleration methods.

This approach consists of first creating a microbunch or train of microbunches using the laser-driven mechanism, e.g., IFEL. The microbunches are spaced apart by a length $\lambda_{\rm accel}$, where $\lambda_{\rm accel}$ is either the laser or plasma wavelength. The microbunch length is also very short, typically $\sim \lambda_{\rm accel}/10$, which means the microbunch(es) are in a configuration that allows them to be trapped and accelerated in subsequent laser-driven stages.

This paper describes an experiment to apply the STELLA approach to a plasma-based acceleration scheme, specifically LWFA. The experiment is called STELLA-laser wakefield (STELLA-LW). This experiment is motivated by the fact that IFELs have inherent scaling limitations and, in particular, become inefficient as the energy of the e-beam increases. In contrast, LWFA has more favorable scaling characteristics and offers the possibility of much higher acceleration gradients than IFELs.

The next section describes the STELLA-LW experiment and predicted results. Conclusions are given in Section III, as well as implications of this experiment and possible future work.

Manuscript received July 16, 2004; revised September 8, 2004. This work was supported by the U.S. Department of Energy under Grants DE-FG02-04ER41294, DE-AC02-98CH10886, and DE-FG03-92ER40695.

W. D. Kimura, C. E. Dilley, and S. C. Gottschalk are with STI Optronics, Inc., Bellevue, WA 98004-1495 USA (e-mail: wkimura@stioptronics.com).

N. E. Andreev, S. V. Kuznetsov, and A. A. Pogosova are with the Institute for High Energy Densities, Russian Academy of Sciences, Moscow 125412, Russia.

M. Babzien, I. Ben-Zvi, K. P. Kusche, I. V. Pavlishin, I. V. Pogorelsky, and V. Yakimenko are with the Brookhaven National Laboratory, Upton, NY 11973 USA.

D. B. Cline and F. Zhou are with the University of California at Los Angeles, Los Angeles, CA 90095 USA.

S. M. Hooker is with the University of Oxford, Oxford OX1 3PU, U.K.

L. C. Steinhauer is with the Redmond Plasma Physics Laboratory, University of Washington, Redmond, WA 98052 USA.

A. Ting is with the Naval Research Laboratory, Washington, DC 20375 USA.

A. Zigler is with the Racah Institute of Physics, The Hebrew University, Jerusalem 91904, Israel.

Digital Object Identifier 10.1109/TPS.2004.841173

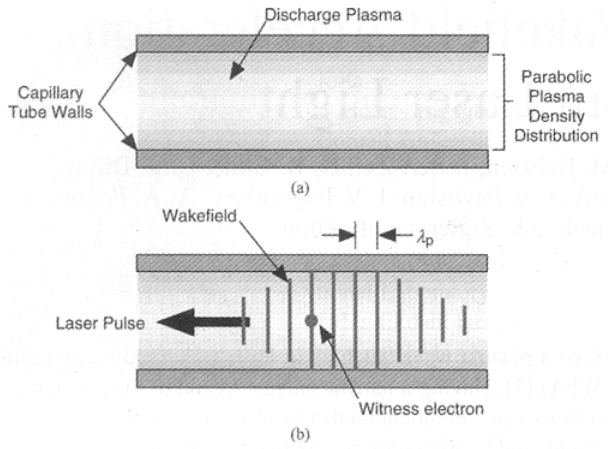

Fig. 1. Basic scheme for resonant laser wakefield acceleration (LWFA). (a) Prepare appropriate plasma with parabolic density distribution for channeling laser light. (b) Send laser pulse through plasma, which creates wakefield behind laser pulse. Properly phased witness electron can then be accelerated by the wakefield.

II. Description of STELLA-LW Experiment

A. Pseudoresonant LWFA

In a typical LWFA experimental arrangement, the *e*-beam and laser beam interact within a plasma as illustrated in Fig. 1. This plasma might be formed using a gas jet [5], a laser beam focused by an axicon in a gas [6], or a capillary discharge [7]. If the plasma density distribution has the proper characteristics [see Fig. 1(a)], it can also channel the laser beam [8]. Without this channeling effect, a tightly focused laser beam could not be maintained longer than a Rayleigh length.

The laser beam excites a wakefield in the plasma, which can be made to travel close to the speed of light c. This wakefield consists of a plasma wave with alternating concentrations of negative and positive charge; see Fig. 1(b). The *e*-beam electrons sense these charges. Depending on the electron's phase position in this wakefield, it can be accelerated or decelerated. Thus, the wakefield has many of the same basic characteristics as the laser field in an IFEL. If electrons are distributed over all phases of the wakefield, then their energy will be modulated just as in an IFEL buncher. If the electrons are concentrated in a microbunch whose longitudinal and transverse size is small enough, these electrons can be trapped and accelerated by the wakefield. Key differences are the wakefield is capable of much higher acceleration gradients than IFELs and there can be strong radial focusing forces on the *e*-beam.

There are two well-known modes of LWFA operation. The first is resonant LWFA, where the laser pulse length $\tau_{\rm L} \sim \lambda_{\rm p}/2c$, where $\lambda_{\rm p}$ is the plasma wavelength. The short laser pulse resonantly excites a wakefield in the plasma because its primary Fourier component matches the plasma frequency. The plasma wavelength is related to the plasma density n_e via

$$\lambda_{\rm p}(\mu{\rm m}) \sim \frac{(3.3 \times 10^{10})}{\sqrt{n_e\,({\rm cm}^{-3})}}. \tag{1}$$

The second mode of operation is self-modulated LWFA (SM-LWFA), in which the laser pulse length is intentionally much longer than $\lambda_{\rm p}/2c$. This permits the laser electric field to feed energy into a wakefield via forward Raman scattering (FRS) and/or self-modulation instability. Much higher gradients are possible using SM-LWFA. However, it starts from noise and becomes a highly nonlinear process, which may interfere with control of the wakefield phase.

LWFA experiments to date have primarily concentrated on studying the basic mechanism and have typically been performed using 0.8–1-μm laser wavelengths, where terawatt-level (TW-level) lasers are readily available. The STELLA-LW experiment will be one of the first to investigate LWFA using 10.6-μm laser wavelength. This is made possible by recent upgrades to the Brookhaven National Laboratory Accelerator Test Facility (ATF) CO_2 laser, which is presently able to produce near-terawatt peak power levels with 10-ps pulse length. Eventually, the ATF CO_2 laser should produce pulses as short as ≈ 2 ps.

Wakefield generation at long laser wavelengths has certain inherent advantages [9]. One is that the normalized laser field parameter a is proportional to the laser wavelength $\lambda_{\rm L}$ (i.e., $a \equiv eE_{\rm L}/\omega mc$, where e is the electron charge, $E_{\rm L}$ is the laser electric field, ω is the laser frequency, and m is the electron mass). This means for the same laser beam focus area, 10-μm light will provide a factor of 10 increase in a compared to 1-μm laser light, and a 100 times increase in the ponderomotive potential, which scales as a^2. While it is true that 1-μm light can be focused to a smaller area than 10-μm light to compensate for this effect, the minimum usable laser beam size is limited by the minimum *e*-beam size that can be obtained. The *e*-beam size depends on other factors, such as the *e*-beam emittance and space charge spreading. From an experimental viewpoint, larger *e*-beam sizes are generally favored because these limitations are eased. Hence, LWFA at 10.6 μm has certain practical advantages.

Theoretical analysis of LWFA driven by 10.6-μm laser light has already been performed [10]–[12]. For the anticipated conditions of the ATF TW CO_2 laser (i.e., ~ 2 ps pulse length, 5 J/pulse), an electric field gradient of ~ 1 GV/m is predicted. This is for $n_e \sim 10^{16}$ cm^{-3}, which is higher than the usual density required to satisfy the resonant condition for a 2-ps laser pulse. Even more noteworthy is this high gradient arises from a strong wakefield that is created despite the fact the 2-ps laser pulse is too long for resonant LWFA and too short for SM-LWFA. It was found that interaction of the laser light with the plasma causes pulse steepening to occur at the trailing edge of the light pulse. This effectively initiates the wakefield generation as if the laser pulse length were much shorter, but the pulse terminates before FRS can play a significant role. Nevertheless, the wakefields produced can be comparable to those formed by SM-LWFA with a longer pulse.

A model simulation [12] of the laser pulse steepening effect and subsequent wakefield generation at 5.5 cm into the plasma is shown in Fig. 2. Plotted is the laser pulse temporal profile with and without the steepening effect, where the former also displays an increase in height.

In Fig. 2, the change in wakefield potential $\delta\Phi = \Phi - 1$ is plotted, where Φ is the scalar potential of the wakefield normalized by e/mc^2. A significant wake trails after the laser pulse, but the laser pulse terminates before appreciable interaction occurs between the laser pulse and the evolving wake.

We refer to this operating regime as pseudoresonant LWFA because the laser pulse effectively acts like a shorter pulse that

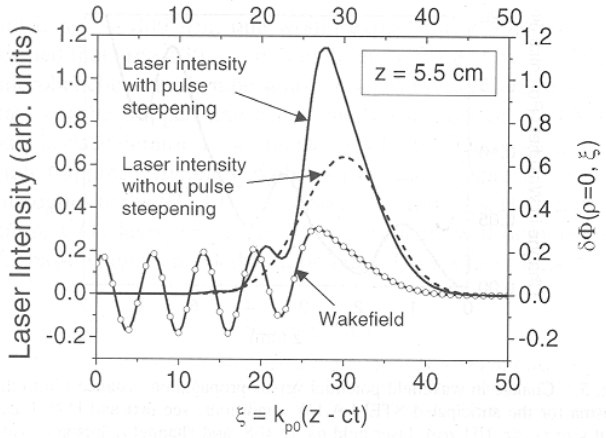

Fig. 2. Laser pulse intensity and change in wakefield potential $\delta\Phi$ on axis (lines marked by circles) at propagation distance $z = 5.5$ cm into the plasma versus the dimensionless coordinate $\xi = k_{\rm p0}(z - ct)$, where $k_{\rm p0} = (4\pi e^2 N_0/m)^{1/2}/c$, e is electron charge, N_0 is the unperturbed electron plasma density, m is the electron mass, and t is time [12]. Dashed curve is the laser intensity without pulse steepening, and the solid curve is with pulse steepening.

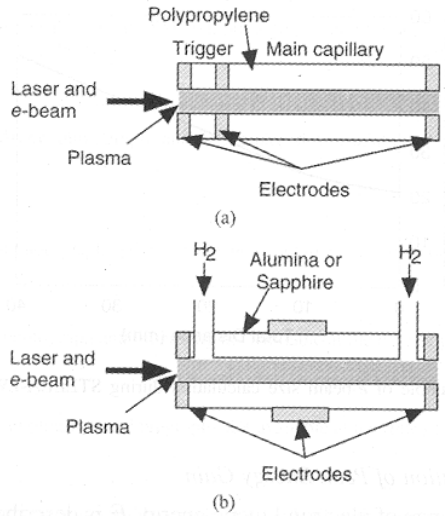

Fig. 3. (a) Schematic of polypropylene capillary discharged based upon [7]. (b) Diagram of gas-filled capillary discharge based upon [15].

would occur in resonant LWFA. This pulse-steepening phenomenon was also independently uncovered in [13], published at the same time as [12].

Because the laser pulse terminates before significant FRS growth occurs, aspects of SM-LWFA that are difficult to control may be mitigated. Thus, the wake produced in the pseudoresonant regime may be more controllable, which would make it easier to stage the LWFA process.

B. Capillary Discharge

STELLA-LW will use a capillary discharge to make the plasma channel because of prior experience at the ATF with capillary discharges [14]. There are two basic types of capillary discharges that can be used. The ATF used the ablative wall technique, where the plasma is generated by discharge-induced ablation of the polypropylene capillary wall material [7]. Fig. 3(a) shows a schematic of the polypropylene capillary discharge.

A second capillary technique [15] uses an alumina or sapphire capillary channel rather than polypropylene. Hydrogen gas is injected into the capillary to provide the medium for the plasma discharge. This method has the advantage of a longer capillary lifetime compared to the ablative method, and the ability to control the plasma density by the amount of gas ejected into the tube. Fig. 3(b) illustrates this gas-filled capillary approach.

A plasma density of $\sim 10^{16}$ cm^{-3} is low enough to avoid absorption of the infrared radiation by the plasma. In addition, the wakefield damping time is inversely proportional to the plasma density with a damping time of ~ 100 ps for 10^{16}cm^{-3} densities. This provides plenty of time for a witness electron pulse to follow the laser pulse and be accelerated by the wakefield.

Nonetheless, achieving a stable and reliable low density of 10^{16} cm^{-3} may be an issue. Generally, capillary discharges have produced plasma densities $\sim 10^{18} - 10^{19}$ cm^{-3}, but this is primarily because these are the densities required for subpicosecond LWFA experiments performed using solid-state lasers.

In a polypropylene capillary discharge, n_e depends on the discharge current I and capillary tube inner radius $R_{\rm cap}$, i.e., $n_e \sim IR_{\rm cap}^{-2}$ [7]. This effect was demonstrated during the ATF channeling experiment where the 1-mm-diameter capillary produced $n_e \sim 10^{17}$ cm^{-3} [14]. Thus, $\sim 10^{16}$-cm^{-3} density might be achievable by increasing the capillary tube inner radius.

However, it may be easier to achieve 10^{16} cm^{-3} density with a gas-filled capillary by simply injecting an appropriate quantity of gas. This helps decouple the plasma density from the capillary dimensions. This is important because the capillary diameter also affects the shape of the parabolic plasma profile, which determines the laser beam size that can be guided and, therefore, the laser intensity in the plasma.

The length of the capillary discharge is a more flexible quantity. In general, longer plasma lengths yield higher energy gains. However, the wakefield also has strong radial focusing components, which can defocus the *e*-beam passing through the plasma. One way to avoid these focusing forces is to tightly focus the *e*-beam inside the center of the plasma channel where the radial field gradient is small. The maximum transverse size of the *e*-beam to avoid radial focusing depends on the wakefield channel characteristics. In [14], the plasma channel radius (radius of density doubling) was 200–250 μm. Based upon earlier preliminary analysis, it appears the *e*-beam diameter should be $\sim 5\times$ smaller than the wakefield diameter to avoid the radial forces. This implies an *e*-beam diameter of ~ 40 μm may be needed.

The ATF has demonstrated *e*-beam focusing down to a spot size of ≈ 15 μm-rms. However, this small diameter can only be maintained over a limited distance. Fig. 4 shows an example simulation of the *e*-beam size versus distance for the STELLA-LW experiment. We see the *e*-beam diameter is ≤ 40 μm if the plasma length is < 3 cm.

Detection of the wakefield inside the capillary discharge will be done utilizing coherent Thomson scattering (CTS) [16]. This diagnostic has been used extensively in plasma-based laser acceleration experiments [17] and [18], but not in capillary discharges. Hence, STELLA-LW will also be one of the first to use CTS on a capillary discharge.

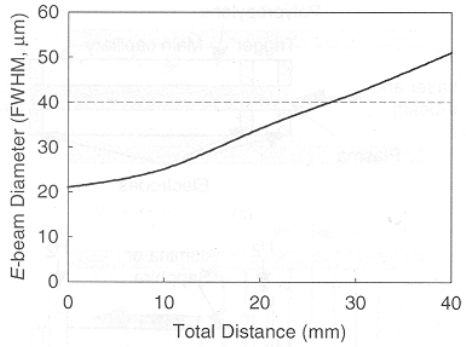

Fig. 4. Example of e-beam size calculation during STELLA-LW focusing conditions.

C. Estimation of Peak Energy Gain

The change of electron kinetic energy E is described by the equation

$$\frac{dE}{dt} = e\mathbf{E}_a\mathbf{v} \tag{2}$$

where $\mathbf{E}_a$ is the accelerating electric field strength and $\mathbf{v}$ is the velocity. For one-dimensional motion (z– axis $\|\mathbf{E}_a$) of an ultrarelativistic electron with a velocity near the speed of light ($|\mathbf{v}| \cong c$), it follows from (2) that the energy gain ΔE during a time T is equal to

$$\Delta E \cong \int_0^{L=cT} eE_a dz. \tag{3}$$

If the wakefield potential has the form

$$\Phi = \Phi_0(z)\sin(k_\mathrm{p}\xi), \quad \xi = z - V_{ph}t \tag{4}$$

where V_{ph} is the phase velocity of the wake wave, $k_\mathrm{p} = 2\pi/\lambda_\mathrm{p}$ is the plasma wave vector, and the characteristic space scale of the wakefield potential amplitude $\Phi_0(z)$ is much longer than the space scale k_p^{-1} of the plasma wave, then $E_a \cong \partial\Phi/\partial\xi$ and from (3) and (4), one can get

$$\Delta E \cong \int_0^L e\Phi_0(z)k_\mathrm{p}\cos(k_\mathrm{p}\xi)dz. \tag{5}$$

For our experimental conditions, we can assume the length of acceleration L is much less than the maximum acceleration length L_max, i.e., $L \ll L_\mathrm{max} = \lambda_\mathrm{L}\gamma_{ph}^3/2$, where γ_{ph} is the Lorentz factor for the wake. This means the change of the phase during the acceleration is small and $\cos(k_\mathrm{p}\xi) \cong 1$. Then, for an electron placed at the maximum of the accelerating field, it follows from (5)

$$\Delta E_\mathrm{max} \cong \int_0^L e\Phi_0(z)k_\mathrm{p}dz = mc^2\int_0^L \varphi_0(z)k_\mathrm{p}dz \tag{6}$$

where $\varphi_0 = e\Phi_0/(mc^2)$ is the dimensionless amplitude of the wakefield potential.

For the parameters modeled in [14], i.e., $\lambda_\mathrm{L} = 10.6\ \mu$m, $\gamma_{ph} = 30$, $k_\mathrm{p} \approx 198\ \mathrm{cm}^{-1}$, $L_\mathrm{max} = 14.3$ cm, (6) gives

$$\Delta E_\mathrm{max}[\mathrm{MeV}] \cong 101\int_0^L \varphi_0(z)dz \tag{7}$$

where L is in centimeters. This equation is a good approximation for the results of modeling a constant wakefield amplitude,

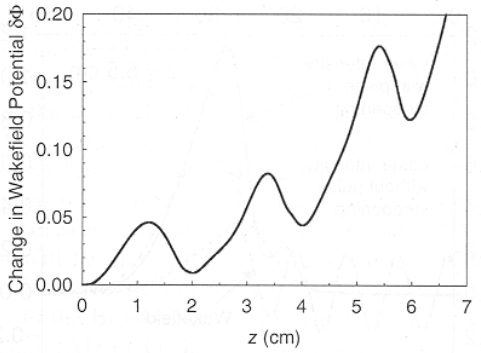

Fig. 5. Change in wakefield potential versus propagation distance z into the plasma for the anticipated STELLA-LW conditions; see text and [12]. Laser spot size $r_\mathrm{L} = 101\ \mu$m, laser field $a_0 = 0.8$, and channel radius at density doubling $R_\mathrm{ch} = 202\ \mu$m.

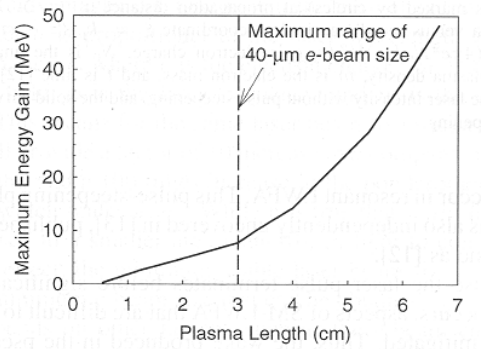

Fig. 6. Maximum energy gain versus plasma length from (7) and integration of the wakefield potential curve in Fig. 5. Also shown is the maximum plasma length over which an e-beam diameter of $\leq 40\ \mu$m can be maintained.

and can be used to estimate the maximum energy gain for the more realistic case when the wakefield oscillates with distance.

Due to the dynamics of the interactions of the wakefield with the laser field inside the plasma, the wakefield potential oscillates as it grows with distance z. This is illustrated in Fig. 5 [12]. The area under the curve shown in Fig. 5 as a function of L yields the integral term in (7). Thus, a plot of (7) can be constructed showing the maximum energy gain versus the plasma interaction length. This is given in Fig. 6.

For a 3-cm length, as limited by the 40-μm e-beam diameter, we predict a maximum acceleration of $\approx$ 8 MeV ($\sim$ 18% energy gain), corresponding to an acceleration gradient of $\approx$ 270 MeV/m. While modest compared to other LWFA experiments, this gradient is still several times higher than microwave systems and sufficient as a proof-of-principle demonstration of pseudoresonant LWFA, driven by 10.6-μm light.

III. Conclusion

The STELLA-LW experiment represents an effort to demonstrate several new advances in laser acceleration research. It will explore the new operating regime of pseudoresonant LWFA. It will be one of the first to demonstrate LWFA, driven by 10.6-μm laser light, and to use CTS on a capillary discharge.

STELLA-LW also represents the first phase of a longer-term program to apply the STELLA approach to LWFA. Possible future experiments include demonstrating a LWFA buncher.

Since $\lambda_p \sim 300\ \mu m$, one would expect microbunches to be formed that are $\sim 30\ \mu m$ in length and separated by λ_p. These microbunches can then be sent into a LWFA accelerator where they can be trapped and accelerated. The goal of the LWFA buncher/accelerator experiments would be demonstration of high trapping efficiency with narrow energy spread, exactly analogous to the STELLA experiment with IFELs. Hence, these future CO_2-laser-driven LWFA experiments will demonstrate the basic features needed by a practical LWFA laser linac.

REFERENCES

[1] C. E. Clayton and P. Muggli, Eds., *Advanced Accelerator Concepts*. ser. AIP Conf. Proc., No. 647. New York: Amer. Inst. Physics, 2002.

[2] E. D. Courant, C. Pellegrini, and W. Zakowicz, "High-energy inverse free-electron-laser accelerator," *Phys. Rev. A, Gen. Physics*, vol. 32, pp. 2813–2823, 1985.

[3] L. M. Gorbunov and V. I. Kirsanov, "Excitation of plasma waves by an electromagnetic wave packet," *Sov. Phys.—JETP*, vol. 66, pp. 290–294, 1987.

[4] W. D. Kimura, M. Babzien, I. Ben-Zvi, L. P. Campbell, D. B. Cline, C. E. Dilley, J. C. Gallardo, S. C. Gottschalk, K. P. Kusche, R. H. Pantell, I. V. Pogoresky, D. C. Quimby, J. Skaritka, L. C. Steinhauer, V. Yakimenko, and F. Zhou, "First demonstration of high-trapping efficiency and narrow energy spread in a laser-driven accelerator," *Phys. Rev. Lett.*, vol. 92, p. 054 801, 2004.

[5] R. Wagner, S.-Y. Chen, A. Maksimchuk, and D. Umstadter, "Electron acceleration by a laser wakefield in a relativistically self-guided channel," *Phys. Rev. Lett.*, vol. 78, pp. 3125–3128, 1997.

[6] S. P. Nikitin, I. Alexeev, J. Fan, and H. M. Milchberg, "High efficiency coupling and guiding of intense femtosecond laser pulses in preformed plasma channels in an elongated gas jet," *Phys. Rev. E, Stat. Phys. Plasmas Fluids Relat. Interdiscip. Top.*, vol. 59, pp. R3839–R3842, 1999.

[7] D. Kaganovich, P. V. Sasorov, Y. Ehrlich, C. Cohen, and A. Zigler, "Investigations of double capillary discharge scheme for production of wave guide in plasma," *Appl. Phys. Lett.*, vol. 71, pp. 2925–2927, 1997.

[8] D. Kaganovich, P. Sasorov, C. Cohen, and A. Zigler, "Variable profile capillary discharge for improved phase matching in a laser wakefield accelerator," *Appl. Phys. Lett.*, vol. 75, pp. 772–774, 1999.

[9] I. V. Pogorelsky, "Prospects for laser wakefield accelerators and colliders using CO_2 laser drivers," *Nucl. Instrum. Methods Phys. Res. A*, vol. 410, pp. 524–531, 1998.

[10] N. E. Andreev, S. V. Kuznetsov, and I. V. Pogorelsky, "Monoenergetic laser wakefield acceleration," *Phys. Rev. ST–Accel. Beams*, vol. 3, p. 021 301, 2000.

[11] S. V. Bulanov, T. J. Esirkepov, N. M. Naumova, F. Pegoraro, I. V. Pogorelsky, and A. M. Pukhov, "Controlled wake field acceleration via laser pulse shaping," *IEEE Trans. Plasma Sci.*, vol. 24, no. 2, pp. 393–399, Apr. 1996.

[12] N. E. Andreev, S. V. Kuznetsov, A. A. Pogosova, L. C. Steinhauer, and W. D. Kimura, "Modeling of laser wakefield acceleration at CO_2 laser wavelengths," *Phys. Rev. ST—Accel. Beams*, vol. 6, p. 041 301, 2003.

[13] Z. Najmudin, K. Krushelnick, E. L. Clark, S. P. D. Mangles, B. Walton, A. E. Dangor, S. Fritzler, V. Malka, E. Lefebvre, D. Gordon, F. S. Tsung, and C. Joshi, "Self-modulated wakefield and forced laser wakefield acceleration of electrons," *Phys. Plasmas*, vol. 10, pp. 2071–2077, 2003.

[14] I. V. Pogorelsky, I. V. Pavlishin, I. Ben-Zvi, T. Kumita, Y. Kamiya, T. Hirose, B. Greenberg, D. Kaganovich, A. Zigler, N. Andreev, N. Bobrova, and P. Sasorov, "Transmission of high-power CO_2 laser pulses through a plasma channel," *Appl. Phys. Lett.*, vol. 83, pp. 3459–3461, 2003.

[15] A. Butler, D. J. Spencer, and S. M. Hooker, "Guiding of high-intensity laser pulses with a hydrogen-filled capillary discharge waveguide," *Phys. Rev. Lett.*, vol. 89, p. 185 003, 2002.

[16] C. V. Filip, S. Y. Tochitsky, R. Narang, C. E. Clayton, K. A. Marsh, and C. J. Joshi, "Collinear Thomson scattering diagnostic system for the detection of relativistic waves in low-density plasmas," *Rev. Sci. Instrum.*, vol. 74, pp. 3576–3578, 2000.

[17] C. E. Clayton, C. Joshi, C. Darrow, and D. Umstadter, "Relativistic plasma-wave excitation by collinear optical mixing," *Phys. Rev. Lett.*, vol. 54, pp. 2343–2346, 1985.

[18] A. Ting, K. Krushelnick, C. I. Moore, H. R. Burris, E. Esarey, J. Krall, and P. Sprangle, "Temporal evolution of self-modulated laser wakefields measured by coherent Thomson scattering," *Phys. Rev. Lett.*, vol. 77, pp. 5377–5380, 1996.

W. D. Kimura (S'75–M'80–SM'91), photograph and biography not available at the time of publication.

N. E. Andreev photograph and biography not available at the time of publication.

M. Babzien photograph and biography not available at the time of publication.

I. Ben-Zvi photograph and biography not available at the time of publication.

D. B. Cline photograph and biography not available at the time of publication.

C. E. Dilley photograph and biography not available at the time of publication.

S. C. Gottschalk photograph and biography not available at the time of publication.

S. M. Hooker photograph and biography not available at the time of publication.

K. P. Kusche photograph and biography not available at the time of publication.

S. V. Kuznetsov photograph and biography not available at the time of publication.

I. V. Pavlishin photograph and biography not available at the time of publication.

I. V. Pogorelsky photograph and biography not available at the time of publication.

A. A. Pogosova photograph and biography not available at the time of publication.

L. C. Steinhauer photograph and biography not available at the time of publication.

A. Ting photograph and biography not available at the time of publication.

V. Yakimenko photograph and biography not available at the time of publication.

A. Zigler photograph and biography not available at the time of publication.

F. Zhou photograph and biography not available at the time of publication.